Punctuated Evolution of Prostate Cancer Genomes

Sylvan C. Baca,[1,2,3] Davide Prandi,[6] Michael S. Lawrence,[2] Juan Miguel Mosquera,[8] Alessandro Romanel,[6] Yotam Drier,[2,7] Kyung Park,[8] Naoki Kitabayashi,[8] Theresa Y. MacDonald,[8] Mahmoud Ghandi,[2] Eliezer Van Allen,[2,3] Gregory V. Kryukov,[1,2,13] Andrea Sboner,[8,9] Jean-Philippe Theurillat,[2] T. David Soong,[9] Elizabeth Nickerson,[2] Daniel Auclair,[2] Ashutosh Tewari,[10,11] Himisha Beltran,[12] Robert C. Onofrio,[2] Gunther Boysen,[8] Candace Guiducci,[2] Christopher E. Barbieri,[8,11] Kristian Cibulskis,[2] Andrey Sivachenko,[2] Scott L. Carter,[2] Gordon Saksena,[2] Douglas Voet,[2] Alex H. Ramos,[1,2] Wendy Winckler,[2] Michelle Cipicchio,[2] Kristin Ardlie,[2] Philip W. Kantoff,[1,3] Michael F. Berger,[14] Stacey B. Gabriel,[2] Todd R. Golub,[2,4,5,15] Matthew Meyerson,[1,2,3,4] Eric S. Lander,[1,2,16,17] Olivier Elemento,[9] Gad Getz,[2] Francesca Demichelis,[6,9,18,*] Mark A. Rubin,[8,11,18] and Levi A. Garraway[1,2,3,4,18,*]

[1]Harvard Medical School, Boston, MA 02115, USA
[2]The Broad Institute of Harvard and MIT, Cambridge, MA 02142, USA
[3]Department of Medical Oncology
[4]Center for Cancer Genome Discovery
[5]Department of Pediatric Oncology
Dana-Farber Cancer Institute, Boston, MA 02215, USA
[6]Centre for Integrative Biology, University of Trento, Povo, Trento 38123, Italy
[7]Department of Physics of Complex Systems, Weizmann Institute of Science, Rehovot 76100, Israel
[8]Department of Pathology and Laboratory Medicine
[9]Institute for Computational Biomedicine, Department of Physiology and Biophysics
[10]Lefrak Center of Robotic Surgery and Center for Prostate Cancer Research & Clinical Care
[11]Brady Foundation Department of Urology
[12]Department of Medicine, Division of Hematology and Medical Oncology
Weill Cornell Medical College, New York, NY 10065, USA
[13]Division of Genetics, Brigham and Women's Hospital, Boston, MA 02115, USA
[14]Department of Pathology, Memorial Sloan-Kettering Cancer Center, New York, NY 10065, USA
[15]Howard Hughes Medical Institute, Chevy Chase, MD 20815, USA
[16]Department of Biology, MIT, Cambridge, MA 02139, USA
[17]Whitehead Institute for Biomedical Research, Cambridge, MA 02142, USA
[18]These authors contributed equally to this work
*Correspondence: demichelis@science.unitn.it (F.D.), levi_garraway@dfci.harvard.edu (L.A.G.)
http://dx.doi.org/10.1016/j.cell.2013.03.021

SUMMARY

The analysis of exonic DNA from prostate cancers has identified recurrently mutated genes, but the spectrum of genome-wide alterations has not been profiled extensively in this disease. We sequenced the genomes of 57 prostate tumors and matched normal tissues to characterize somatic alterations and to study how they accumulate during oncogenesis and progression. By modeling the genesis of genomic rearrangements, we identified abundant DNA translocations and deletions that arise in a highly interdependent manner. This phenomenon, which we term "chromoplexy," frequently accounts for the dysregulation of prostate cancer genes and appears to disrupt multiple cancer genes coordinately. Our modeling suggests that chromoplexy may induce considerable genomic derangement over relatively few events in prostate cancer and other neoplasms, supporting a model of punctuated cancer evolution. By characterizing the clonal hierarchy of genomic lesions in prostate tumors, we charted a path of oncogenic events along which chromoplexy may drive prostate carcinogenesis.

INTRODUCTION

Though often curable at early stages, clinically advanced prostate cancer causes over 250,000 deaths worldwide annually (Jemal et al., 2011). Identifying prostate cancers that require aggressive treatment and gaining durable control of advanced disease comprise two pressing public health needs. A deeper understanding of the molecular genetic changes that occur during the development of invasive and metastatic tumors may provide useful insights into these problems.

Genetic studies of prostate cancer have revealed numerous recurrent DNA alterations that dysregulate genes involved in prostatic development, chromatin modification, cell-cycle regulation, and androgen signaling, among other processes (Baca and Garraway, 2012). Chromosomal deletions accumulate early in prostate carcinogenesis and commonly inactivate tumor suppressor genes (TSGs) such as *PTEN*, *TP53*, and *CDKN1B* (Shen and Abate-Shen, 2010). In addition, recent exome sequencing of

localized and castration-resistant prostate cancer has identified base-pair mutations in genes such as *SPOP*, *FOXA1*, and *KDM6A*, which implicate a range of deregulated cellular processes in prostate tumor development (Barbieri et al., 2012; Grasso et al., 2012; Kumar et al., 2011).

Structural genomic rearrangements also play a critical role in prostate carcinogenesis. Roughly half of prostatic adenocarcinomas overexpress an oncogenic ETS transcription factor gene (most commonly *ERG*) because of somatic fusion with a constitutively active or androgen-regulated promoter (Tomlins et al., 2007; Tomlins et al., 2005). In addition, disruptive rearrangements may inactivate TSGs such as *PTEN* or *MAGI2* (Berger et al., 2011). Interestingly, analysis of prostate cancer genomes has revealed complex "chains" of rearrangements, which may result when broken DNA ends are shuffled and religated to one another in a novel configuration (Berger et al., 2011). In theory, these DNA-shuffling events could simultaneously dysregulate multiple cancer genes, but the prevalence and consequences of rearrangement chains could not be assessed given the small panel of tumors sequenced.

Given the importance of structural genomic alterations in prostate cancer genesis and progression, we performed whole-genome sequencing (WGS) and DNA copy number profiling of 57 prostate cancers to define a spectrum of oncogenic events that may operate during prostate tumor development. Through computational modeling of rearrangements and copy number alterations, we inferred that the chromosomal disarray in a typical tumor may accumulate over a handful of discrete events during tumor development. We employ the term "chromoplexy" to describe this putative phenomenon of complex genome restructuring (from the Greek *pleko*, meaning to weave or to braid). These complex rearrangement events occur in the majority of prostate cancers and may commonly inactivate multiple tumor-constraining genes in a coordinated fashion. This knowledge informs a model for punctuated tumor evolution relevant to prostate cancer and possibly other malignancies.

RESULTS

The Landscape of Genomic Rearrangement in Prostate Cancer

We sequenced the genomes of 55 primary prostate adenocarcinomas and two neuroendocrine prostate cancer (NEPC) metastases that developed after castration-based therapy as well as paired normal tissue. We selected treatment-naive adenocarcinomas across a range of clinically relevant tumor grades and stages (Gleason score [GS] 6 through 9; pathological stage pT2N0 through pT4N1; Table S1 available online). Roughly 1.68×10^{13} sequenced base pairs aligned uniquely to the hg19 human reference genome (Table S2). Sequencing of tumor and normal DNA to mean coverage depths of 61× and 34×, respectively, revealed 356,136 somatic base-pair mutations with an average of 33 nonsilent exonic mutations per primary tumor (Figure 1 and Table S3A). We profiled somatic copy number alterations (SCNAs) of DNA with high-density oligonucleotide arrays (Table S3B). Additionally, we conducted transcriptome sequencing on 20 tumors, along with matched benign prostate tissue for 16 cases.

To identify genomic rearrangements, we analyzed paired-end sequencing reads that map to the reference genome in unexpected orientations using the dRanger algorithm (Berger et al., 2011). We observed 5,596 high-confidence rearrangements that were absent from normal DNA in both this cohort and an extended panel of 172 noncancerous genome sequences (Figure 1 and Table S3C). We validated 113 rearrangements by resequencing and/or PCR amplification of tumor and normal DNA (Table S3C). We did not discover novel recurrent gene fusions but observed several singleton events that may have led to the overexpression of oncogenes. For example, sense-preserving fusions joined *NRF1* to *BRAF* (PR-4240) and *CRKL* to the ERK-2 kinase gene *MAPK1* (P04-1084; Figure S1A), leaving the kinase-encoding exons of *BRAF* and *MAPK1* primarily intact. Several genes, such as *PTEN*, *RB1*, *GSK3B*, and *FOXO1*, underwent recurrent disruptive rearrangements with potential biological consequence (Figure S1 and Table S4). Thus, rearrangement of these genes may contribute to the development of localized prostate cancer.

DNA Deletions and Rearrangements Reveal Signatures of Complex Genome-Restructuring Events

Rearrangements involving cancer gene loci often occurred in the context of a "chain" in which the two rearrangement breakpoints map to the reference genome near breakpoints from other rearrangements (Figure 2A, left). Such characteristic breakpoint distributions were observed in our initial study of seven prostate cancer genomes (Berger et al., 2011) and appear to reflect collections of broken DNA ends that are shuffled and ligated to one another in an aberrant configuration. Given the involvement of prostate cancer genes in rearrangement chains, we set out to survey chained rearrangements systematically in order to clarify their prevalence and potential biological consequences.

First, we determined whether additional chains could be identified by integrative analysis of chromosomal deletions and rearrangements. Although rearrangement chains may arise with a minimal loss of genetic material, substantial DNA deletions were often evident at the fusion junctions of chained rearrangements (Figure 2A, right). When these deletions are overlaid with somatic rearrangement locations on the reference genome, the deletions create "bridges" that spanned the sequence between breakpoints from two different fusions (Figure 2A, bottom right). In all informative tumors in our cohort, the breakpoints at either end of a deletion were more often fused to novel partners rather than to each other (thus creating "deletion bridges" rather than "simple deletions"; Figure S2A). Importantly, this observation indicates that the many rearrangements demonstrating DNA loss near a breakpoint may be linked by deletion bridges to additional rearrangements in a chain.

Next, we considered whether rearrangements in a chain might arise independently of one another, for instance, at loci that are predisposed toward fusion because of DNA secondary structure or nuclear proximity (Burrow et al., 2010; De and Michor, 2011). To investigate this, we created a probabilistic model for the independent generation of detectable rearrangements across the genome (Figure S2B). Using this model, we
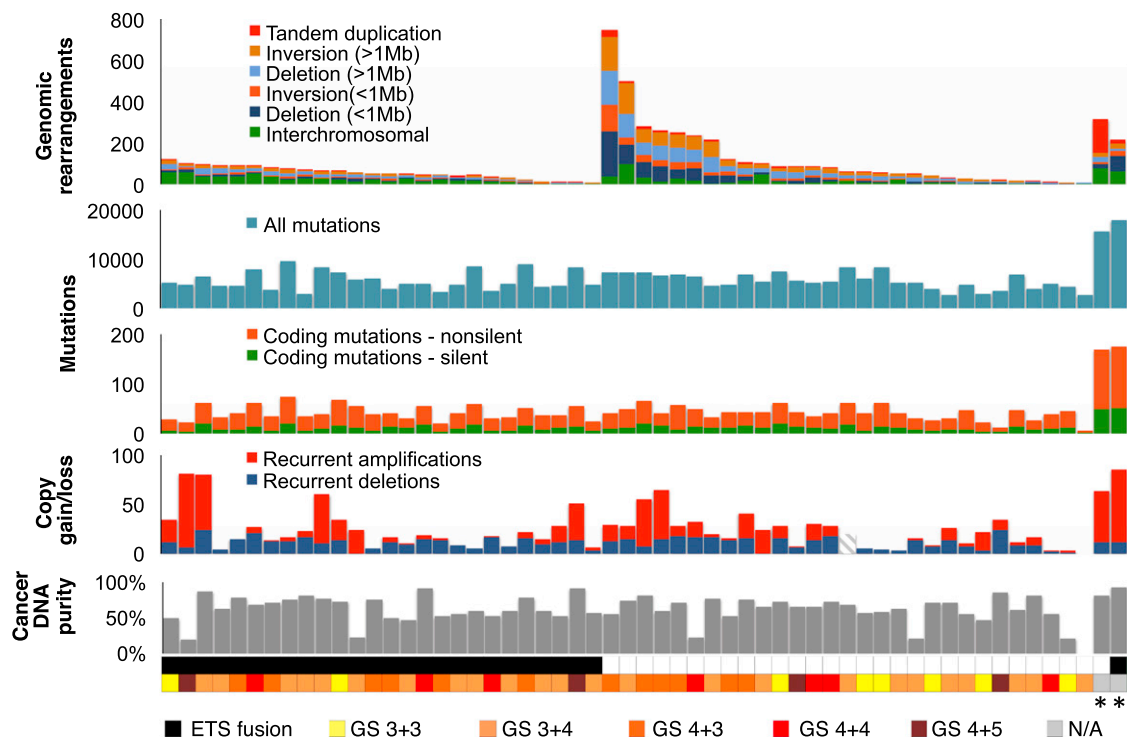
**Figure 1. Somatic Alterations in 57 Prostate Tumor Genomes**

WGS was conducted on 55 prostate adenocarcinomas and two lung metastases from neuroendocrine prostate cancers (NEPC, *) along with paired normal DNA to detect somatic rearrangements and mutations. Gains and losses of DNA copy number at sites of recurrent SNCAs were detected with Affymetrix SNP 6.0 arrays (recurrent SCNAs were not assessed for sample P07-144, hatched lines). Bottom, cancer DNA purity was evaluated by assessing allelic ratios from sequence reads covering heterozygous single-nucleotide polymorphisms at sites of chromosomal deletion (Extended Experimental Procedures). ETS gene fusions (*ERG* and *ETV1*) were detected by sequencing and validated by fluorescence in situ hybridization (FISH).

Also see Tables S1–S4 and Figure S1.

calculated the probability that any pair of neighboring DNA breakpoints X and Y would arise independently of each other (P_{XY}) on the basis of (1) their reference genome distance and (2) the local rate of rearrangements observed in our tumor panel (Figure 2B). As a control, we created ten simulated genomes for each tumor, rearrangement locations being matched for chromosome, local gene expression levels, sequence guanine and cytosine content and DNA replication timing, among other factors (Extended Experimental Procedures). In addition, we generated "scrambled" genomes by combining rearrangements from distinct tumors, preserving locus-specific effects that may promote double strand breakage. The observed rearrangements, but not the simulated or scrambled data, showed a marked deviation from the independent model (Figure S2C) and a statistical enhancement of chain-like patterns (Figure 2B). For 50% of rearrangements, the reference genome locations of both breakpoints were nearer to breakpoints of additional rearrangements than would be expected by chance (p < 10^{-4} for observed versus simulated or scrambled P_{XY} values). To the extent that our model correctly predicts the genomic distribution of independent rearrangements, these results suggest that rearrangement chains are unlikely to arise from independent events, thus raising the hypothesis that they occur by a co-ordinated process.

Chromoplexy Generates Chained Chromosomal Rearrangements and Deletions

Having identified chained patterns of rearrangements that may result from interdependent alterations, we created an algorithm called ChainFinder to search for such events systematically (Figures 3A and S3). ChainFinder employs a statistically based search rooted in graph theory to identify genomic rearrangements and associated deletions that deviate significantly from our independent model described above and, thus, appear to have arisen in an interdependent fashion (Extended Experimental Procedures).

We used ChainFinder to survey our panel of prostate tumors for rearrangement chains. Strikingly, this analysis revealed numerous chains involving widely variable numbers of rearrangements. Some chains involved only three fusions, whereas others contained more than 40 rearrangements that wove five or more chromosomes together (Table S5A and Figures 3B and S3). We have termed the putative process of genomic restructuring that produces these complex chains "chromoplexy." Chromoplexy-related chains of five or more rearrangements (ten or more breakpoints) were detected in 50 out of 57 tumors (88%; Table S5B and Figure S3C), whereas 36 out of 57 tumors (63%) contained two or more such chains. Overall, 39% of rearrangements participated in chains, whereas ChainFinder detected
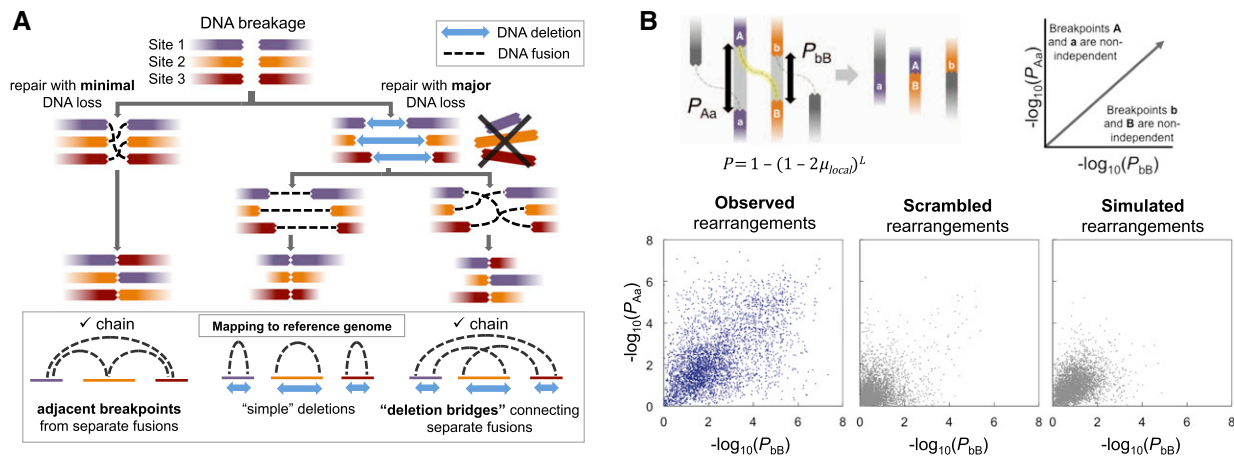
Figure 2. Integrated Analysis of Genomic Deletions and Rearrangements Reveals Signatures of Concurrent Alterations

(A) Three scenarios by which multiple DNA double-strand breaks may be repaired are shown. Concerted repair with minimal loss of DNA (left) results in fusion breakpoints that map to adjacent positions in the reference genome. The loss of DNA at sites of double-strand breaks may result in simple deletions (middle) or deletion bridges (right) that span breakpoints from distinct fusions on the reference genome. Adjacent breakpoints or deletion bridges may provide evidence for chained rearrangements.

(B) For the two breakpoints of each rearrangement (labeled A and B), the probability (P) of a second independently generated breakpoint (labeled a and b) falling within the observed distance (L) was assessed based on the expected local rate of rearrangements (μ_{local}). The x and y coordinates represent the negative log of P for the two breakpoints in each fusion. Rearrangements near the upper right corner of the plot are unlikely to have arisen independently of other rearrangements. Observed rearrangements are compared to simulated and scrambled data.

Also see Figure S2.

chains in only 2.8% and 0.2% of rearrangements from simulated or scrambled genomes, respectively (Figures 3C and 3D). Thus, our statistical analysis of breakpoint distributions suggests that chromoplexy frequently generates multiple structural alterations in a coordinated fashion.

We noted profound phenotypic differences in chromoplexy in subsets of prostate cancers. Chromoplexy in tumors harboring oncogenic ETS fusions (ETS[+]) produced significantly more interchromosomal rearrangements than ETS[−] tumors (p < 10^{−4}) and involved a greater maximum number of chromosomes in a single event (p = 0.009; Figures 4A–4C). Interestingly, oncogenic *ERG* fusions frequently arose in the setting of chromoplexy (15 of 26 cases, 58%). Given that fusion of *TMPRSS2* and *ERG* occurs in the setting of androgen receptor-driven transcription (Haffner et al., 2010), the intricate chains in ETS[+] tumors could reflect DNA injury at transcriptional hubs occupied by loci from multiple chromosomes. Consistent with this possibility, chromoplexy in ETS[+] nuclei primarily affected regions of the genome that were highly expressed in prostate tumors (Figure 4D) and that colocalized in interphase nuclei (Figure S4A). Thus, chromoplexy in ETS[+] tumors appears to reflect a distinct process of genome restructuring that may be coupled to transcriptional processes.

In contrast, chromoplexy in a subset of ETS[−] cancers resembled chromothripsis (Rausch et al., 2012; Stephens et al., 2011), a process of chromatin shattering that yields extensive DNA rearrangement, often of one or two focal chromosomal regions. In particular, seven ETS[−] tumors contained up to 7-fold more rearrangements than the whole-cohort average (Figure S4B). These tumors harbored focal deletions or disruptive rearrangements involving the chromatin-modifying enzyme gene *CHD1*, a putative TSG that may regulate genomic stability (Huang et al.,

2012; Liu et al., 2012). The rearrangements in *CHD1*[del] tumors were predominantly intrachromosomal both within chains (p = 2 × 10^{−4}) and overall (p = 4 × 10^{−4}; Figure S4C). Moreover, the rearrangements in *CHD1*[del] samples arose in late-replicating DNA with low guanine and cytosine content (Figure S4B), generally corresponding to gene-poor heterochromatin. An extended cohort of 199 prostate adenocarcinomas revealed that *CHD1* loss was associated with an increased number of recurrent SCNAs (p = 1.5 × 10^{−8}) (Figure S4C). Given the postulated roles of CHD1 in genome stability and maintenance of chromatin architecture (Gaspar-Maia et al., 2009), these findings raise the possibility that *CHD1* deletion may contribute to the distinctive patterns of genomic instability observed in *CHD1*[del] tumors.

Chromoplexy Commonly Dysregulates Cancer Genes

To assess the role of chromoplexy in prostate cancer development, we examined the genomic regions altered by deletion or disruptive rearrangements in the context of chains. Using a list of 17 potential prostate TSGs from the KEGG database (Kanehisa et al., 2012), we found that 26 of the 57 tumors (46%) had either deletion or rearrangement of at least one gene in a chain of three or more rearrangements (Table S5C). Inclusion of the *TMPRSS2-ERG* fusion and ten putative prostate cancer genes added nine more samples. Several cancer genes were recurrently deleted or rearranged by chromoplexy, including *PTEN* (nine cases), *NKX3-1* (eight cases), *CDKN1B* (three cases), *TP53* (four cases), and *RB1* (two cases). Thus, chromoplexy may conceivably influence prostate carcinogenesis by disrupting TSGs and creating oncogenic fusions.

The concurrent shuffling and deletion of multiple regions across the genome that appears to underlie chromoplexy could
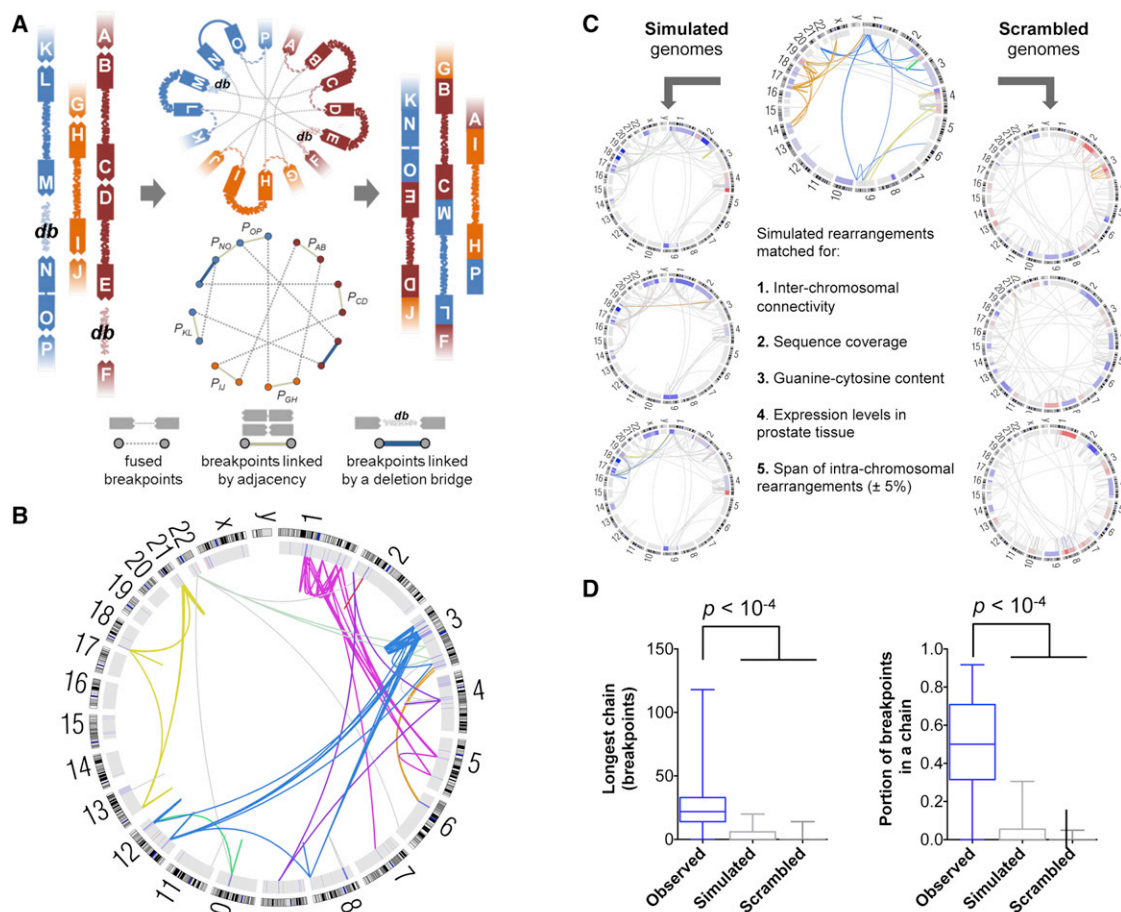
Figure 3. The ChainFinder Algorithm

(A) ChainFinder creates a graphical representation of genomic breakpoints that may be linked in chains by somatic fusions, statistical adjacency, or deletion bridges. ChainFinder assigns two neighboring breakpoints to the same chain if the p value for their independent generation (P) is rejected with a false-discovery rate below 10^{-2}. For each cycle (closed path) within the graph, all scenarios are considered where one or more rearrangements in the cycle could have arisen independently. All rearrangements in a cycle are assigned to the same chain if every such scenario is rejected with a family-wise error rate below 10^{-2} across all scenarios.

See the Extended Experimental Procedures for additional details.

(B) A Circos plot of chained rearrangements in a prostate adenocarcima (P09-1042). Rearrangements depicted in the same color arose within the same chain; fusions in gray were not assigned to a chain. The inner ring depicts copy number gains and losses in blue and red, respectively.

(C) The false-positive rate of ChainFinder was assessed with simulated and scrambled genomes on the basis of observed rearrangements.

(D) For observed, simulated, and scrambled genomes, the longest chain was compared along with the portion of breakpoints in any chain. Median values, middle quartiles, and range are indicated.

Also see Figure S3.

---

simultaneously inactivate TSGs that are geographically distant from each other (i.e., on separate chromosomes). We noted several examples where multiple cancer genes were apparently disrupted by a single instance of chromoplexy. For instance, a chain of 27 rearrangements across six chromosomes included the *TMPRSS2-ERG* fusion (21q) as well as a disruptive rearrangement of the prostate tumor-suppressor gene *SMAD4* (18q) (Ding et al., 2011) (Figures 5A and S5). In a second example, the adjacent *CDKN1B/ETV6* tumor-suppressor genes (12p) and the *ETV3* locus (1q) were lost in the context of deletion bridges within one chain (Figure 5B). Additional instances of chromoplexy disrupted interacting genes in the same pathway; for instance, codeletion of *PIK3R1* (5q) with *PTEN* (10q) and

TP53 (17p) with *CHEK2* (22q) occurred in two chains (Table S5C). Thus, chromoplexy may simultaneously dysregulate multiple cancer genes across the genome. Such events may provide selective advantages to incipient cancer cells, particularly given that the loss of some TSGs promotes prostate cancer only in the context of specific accompanying molecular lesions (Chen et al., 2005).

Clonal Evolution Reveals Paths of Prostate Cancer Progression

To provide additional insight into the genomic evolution of prostate tumors, we analyzed the clonal status of mutations and deletions in our cohort. Using an approach related to previously
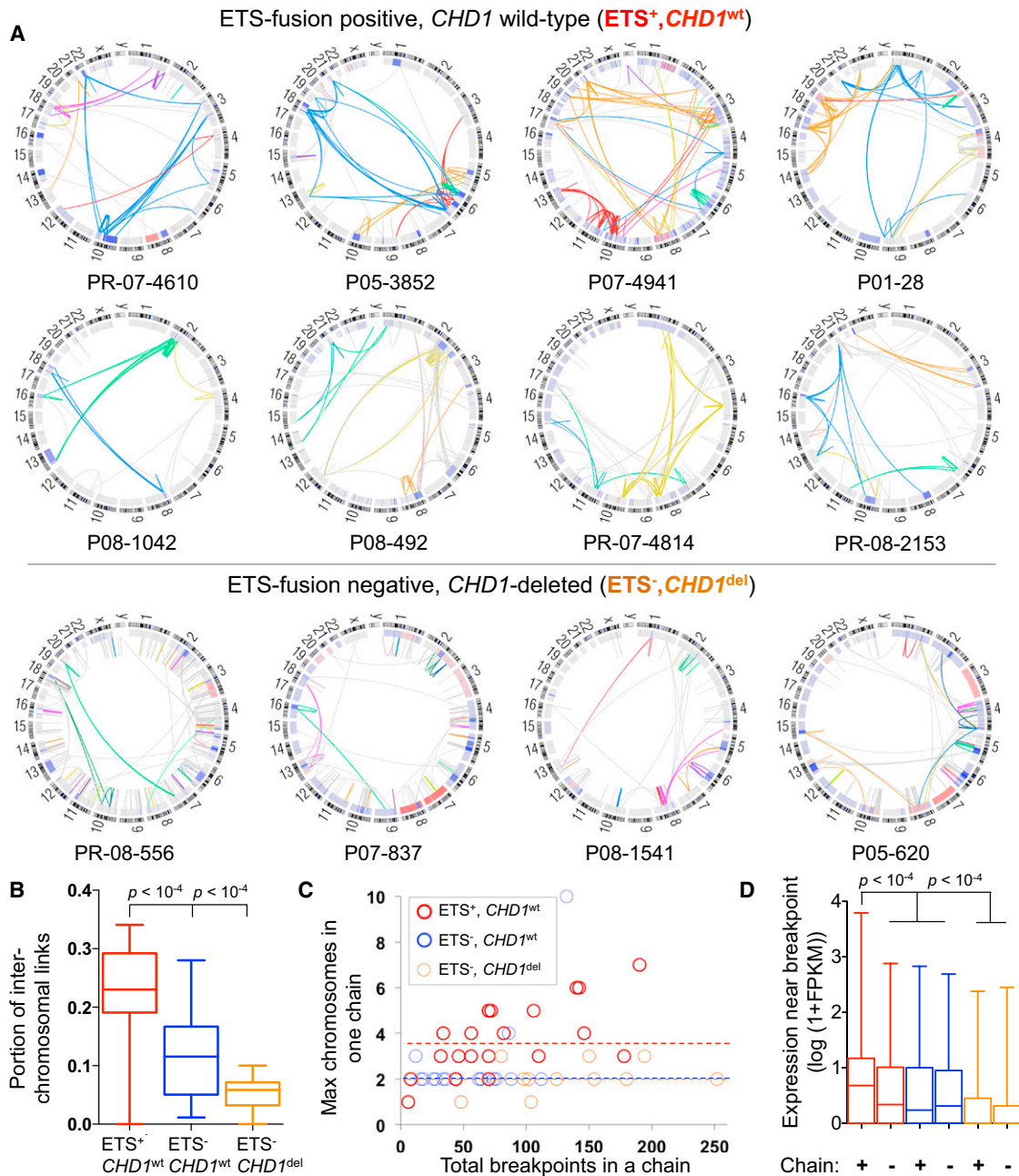
Figure 4. Manifestations of Chromoplexy Vary by ETS Fusion Status

(A) Circos plots of rearrangement chains in representative tumors, grouped by the presence of ETS rearrangements and *CHD1* disruption. Rearrangements in the same chain are depicted in one color. Rearrangements in gray were not assigned to a chain. The inner ring shows copy number gain and loss in red and blue, respectively.

(B) Rearrangement chains in ETS⁺ tumors contain a greater proportion of interchromosomal fusions than chains in ETS⁻ tumors. In (B) and (D), box plots indicate median values, middle quartiles, and range.

(C) The maximum number of chromosomes involved in a single rearrangement chain (y axis), grouped by ETS status. The total number of breakpoints in chains in each tumor is depicted on the x axis to allow comparison of tumors with similar degree of detectable chromoplexy.

(D) ETS⁺ chromoplexy breakpoints are enriched near DNA that is highly expressed in 16 prostate tumor transcriptomes.

Also see Figure S4.

described methods (Carter et al., 2012; Nik-Zainal et al., 2012), we exploited the extensive germline SNP genotype data provided by WGS to assess tumor purity and the clonal status of genomic lesions (Figures 6A and S6). Our estimates of tumor purity based on WGS matched those produced by Absolute analysis of SNP array data (Carter et al., 2012) (R^2 = 0.99;
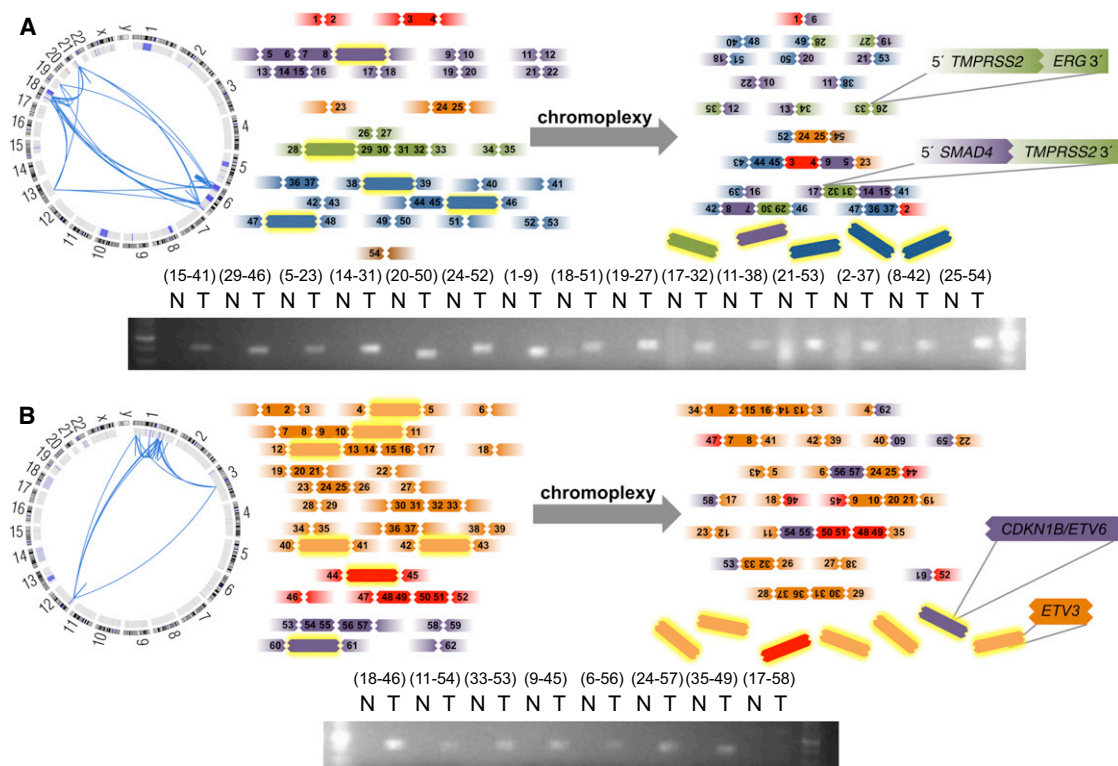
Figure 5. Chromoplexy May Coordinately Dysregulate Multiple Cancer Genes

(A) A chromoplexy-related chain of 27 somatic rearrangements across six chromosomes in tumor P05-3852, involving fusion of *TMPRSS2* and *ERG* and disruptive rearrangement of *SMAD4*.

(B) The putative TSGs *CDKN1B*, *ETV6*, and *ETV3* were lost in the context of deletion bridges in a 25 rearrangement chain affecting three chromosomes in PR-05-3595.

In both panels, selected rearrangements were assessed by PCR of tumor and normal DNA.

Also see Figure S5 and Table S5C.

$p < 10^{-4}$) with the exception of two samples where admixed normal DNA was detected only from sequencing data (Table S1).

First, we compared the clonality of deletions involving prostate cancer genes, reasoning that lesions that arise early in tumorigenesis or that foster rapid outgrowth would tend to be clonal, whereas late-arising deletions would more often be subclonal. Several common deletions were strictly clonal, including *NKX3-1* and the 3Mb region of chromosome 21q that is frequently deleted to produce the *TMPRSS2-ERG* fusion (Perner et al., 2006) (Figures 6B and S6). These events are among the earliest detectable alterations in prostate cancer and are frequently observed in prostatic intraepithelial neoplasia (PIN), a prostate cancer precursor lesion (Emmert-Buck et al., 1995; Perner et al., 2007). By contrast, deletions of *PTEN* were often subclonal ($p = 10^{-5}$ for comparison with *NKX3-1* deletion clonality), as were *CDKN1B* deletions (Figure 6C). This finding suggests that *PTEN* and *CDKN1B* inactivation promotes the early progression of prostate cancer, consistent with the association of these events with higher-stage disease (Barbieri et al., 2012; Halvorsen et al., 2003).

Next, we used our clonality assessments to deconvolve the sequence of oncogenic events that gives rise to a typical prostate tumor. Reasoning that clonal alterations must originate prior to

subclonal alterations within the same tumor, we examined pairs of genes that were deleted in the same sample across multiple tumors to determine the directionality of the clonal-subclonal hierarchy (Figure 6D). Where possible, we confirmed these relationships in independent exome-sequenced tumors. A "consensus path" of progression emerged, beginning with events including the deletion of *NKX3-1* or *FOXP1* and fusion of *TMPRSS2* and *ERG*. These lesions may disrupt normal prostate epithelial differentiation (Bhatia-Gaur et al., 1999; Sun et al., 2008) and affect other oncogenic perturbations. Thereafter, lesions in *CDKN1B* or *TP53* accumulate; these alterations may lead to enhanced proliferation, genomic instability and/or evasion of apoptosis. Finally, loss of *PTEN* may provide a gating event in the development of aggressive prostate cancers. A similar assessment of point mutation clonality (Figure 6B, lower) revealed higher overall rates of subclonal events with the exception of early mutations as in *SPOP* and *FOXA1*. Altogether, these results imply that prostate carcinogenesis favors the dysregulation of cancer genes in defined sequences, as has been suggested by studies of developing tumors in colon cancer (Fearon and Vogelstein, 1990).

Then, we investigated whether chromoplexy might continue after cancer initiation and, thereby, contribute to the progression of a tumor down an oncogenic path. Interestingly, several chains
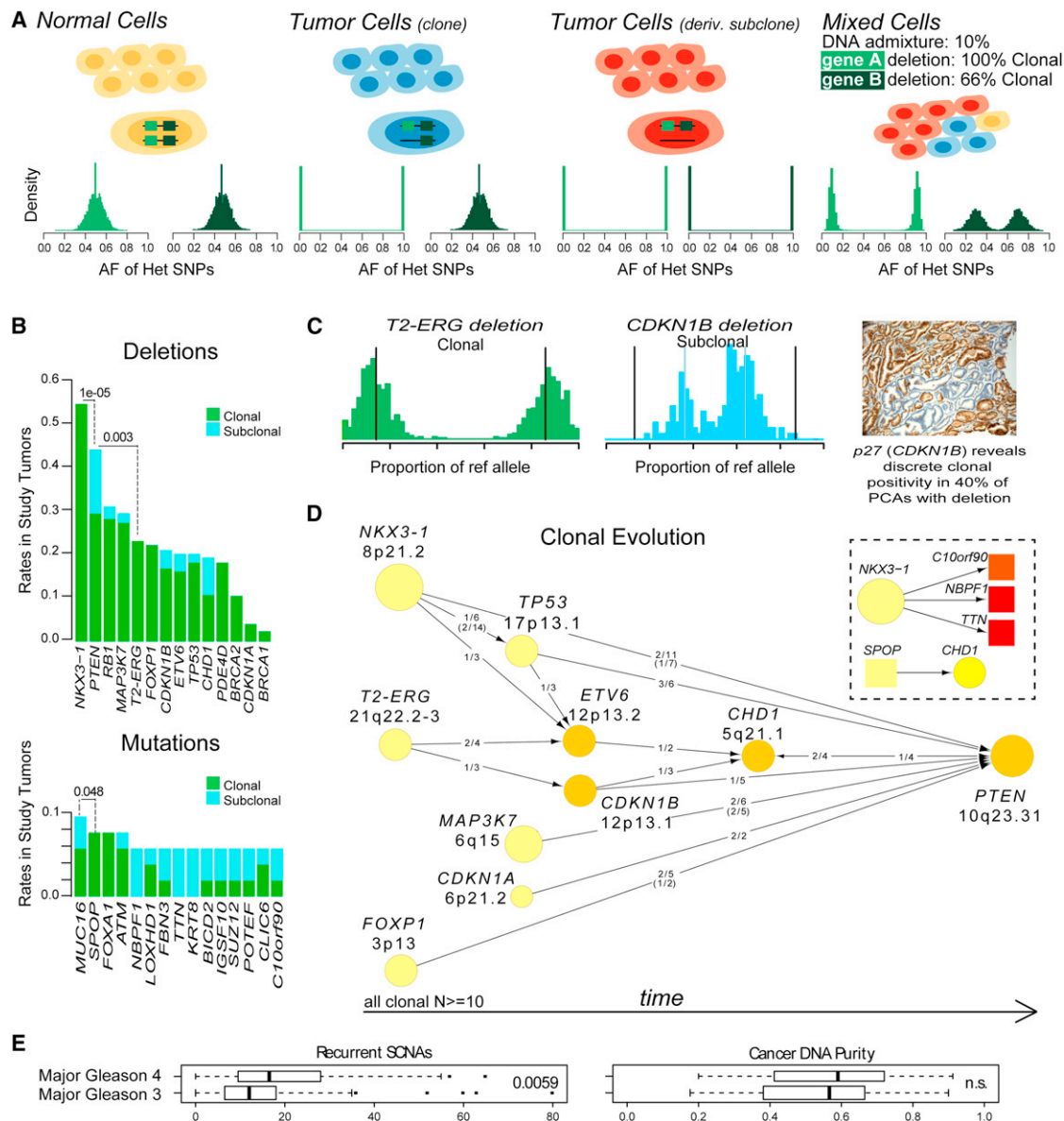
Figure 6. Clonality and Evolution of Prostate Cancer

(A) A schematic representation of the clonality assessment. The allelic fractions (AFs) of sequencing reads covering heterozygous SNPs were analyzed for the assessment of the clonality of somatic DNA alterations. A hypothetical tumor is shown, composed of normal cells, a cancer clone, and a derivative subclone. The histograms indicate the expected SNP AFs within two deleted genes, A and B. The subclonal deletion of B yields a distinct distribution of AFs in comparison to the clonal deletion of A.

(B) Selected deletions (top) and mutations (bottom) were classified as clonal or subclonal. Proportion test p value is listed for the indicated comparisons. Independent samples (Barbieri et al., 2012) are included for support.

(C) An example of clonal (*TMPRSS2-ERG*) and subclonal (*CDKN1B*) deletions from the same tumor. Histograms show the proportion of sequencing reads containing the reference allele for heterozygous SNPs in the deleted regions. A representative immunohistochemical stain for the *CDKN1B* protein p27 shows discrete subclonal positivity in prostate cancer.

(D) Patterns of tumor evolution were inferred on the basis of clonality estimates. Arrows indicate the direction of clonal-subclonal hierarchy between genes that are deleted in the same sample in multiple cases. Deleted genes are represented by circles with size and color intensity reflecting the frequency of overall deletions and subclonal deletions, respectively. Ratios along the arrows indicate the number of samples demonstrating directionality of the hierarchy out of samples with deletion of both genes (ratios in parentheses refer to additional samples; Barbieri et al., 2012). The inset shows a similar analysis of point mutations (Barbieri et al., 2012).

(E) The number of recurrent SCNAs and cancer DNA purity were compared across tumors with major Gleason pattern 4 versus 3. Box plots indicate median values, middle quartiles, and range.

Also see Figure S6.

appeared to involve strictly subclonal deletion bridges (Figure S7A), indicating that tumors may sustain multiple rounds of chromoplexy. Along with the observation that chromoplexy may affect both early and late genes in the consensus path (e.g., *ERG* and *PTEN*), these findings suggest that chromoplexy also occurs in tumor subclones that emerge later during cancer evolution.

Prostate Cancer Genomic Derangement Increases with Histological Grade

Finally, we considered whether tumors with high-grade histology (indicative of high clinical risk) might occupy positions further along the consensus path. To this end, we quantified recurrent SCNAs in each genome by counting amplifications and deletions that overlapped with regions of significant SNCAs identified by GISTICv2 analysis (e.g., the *TP53* and *PTEN* loci) across 199 tumors reported here and in a previous study (Barbieri et al., 2012; Mermel et al., 2011). Tumors with predominantly GS 4 histology were significantly enriched for recurrent SCNAs compared to GS 3 tumors (p = 0.0059; Figure 6E) beyond the overall extent of SCNAs, despite similar purity of cancer DNA and mutational burden between the two groups. Altogether, these findings suggest that structural alterations affecting cancer genes, many of which result from chromoplexy, may contribute to the aggressive clinical behavior of high-grade prostate tumors.

DISCUSSION

We have characterized somatic alterations across the genomes of 57 prostate tumors. By systematically profiling rearrangements and copy number alterations, we identified chromoplexy as a common process by which multiple geographically-distant genomic regions may be disrupted at once. Like other classes of complex genomic alterations (Stephens et al., 2011; Forment et al., 2012), chromoplexy was inferred from computational modeling, and its mechanistic underpinnings will need to be addressed experimentally. Chromoplexy is evident in several solid tumor types and in the majority of prostate cancers. In multiple instances, chromoplexy altered more than one cancer gene coordinately. In the future, systematic assessment of chromoplexy from WGS data could reveal groups of cancer gene alterations that confer a selective advantage when sustained all at once but activate tumor-suppressing safeguards if sustained individually.

Although chained rearrangements could theoretically arise over multiple cellular generations by a "sequential-dependent" mechanism, where the occurrence of each subsequent event depends on the presence of a prior event (Figure S7B), such a mechanism seems unlikely. In particular, a sequential-dependent model fails to account for the many complete or "closed" chains we detected. For a closed chain to arise in a sequential-dependent manner, multiple junctions from ancestral somatic fusions would have to be rebroken precisely and fused to each other (Figure S7B) in order to complete the chain. Even if breakpoints in a chain could only fuse to one another, generating the 121 observed closed chains in a sequential-dependent process would require immensely elevated rates

of rearrangement in a focused region of the genome (up to ~10^3 times the maximum observed rate; Figures S7C and S7D). Although we cannot exclude this possibility, plausible biological mechanism(s) could parsimoniously account for chained rearrangements within a single cell cycle, as discussed below.

A unifying feature of chromoplexy-associated alterations is that they occur in a nonindependent fashion; however multiple mechanisms may account for chromoplexy. Along these lines, our analyses have revealed distinctive patterns of chromoplexy in ETS⁻, *CHD1*ᵈᵉˡ tumors. Tumors with a deletion of *CHD1* demonstrated an excess of intrachromosomal chained rearrangements and gene deletions, DNA breakpoints being enriched in GC-poor, late-replicating, and nonexpressed DNA. Previous reports have proposed that similar patterns may result from major DNA-damaging events within heterochromatic nuclear compartments (Drier et al., 2013). These tumors showed abundant, clustered rearrangements that often affected only one or two chromosomes with two alternating copy number states, perhaps indicating a chromothripsis-like process.

In contrast, chromoplexy in ETS⁺ tumors differed in the aggregate from chromothripsis in several critical ways. For example, single events joined DNA from dispersed regions of six or more chromosomes in multiple tumors, whereas chromothripsis frequently involves focal rearrangement of one or two chromosomes (Forment et al., 2012). Overall, chromoplexy appears more prevalent in ETS⁺ prostate cancer than chromothripsis is in any neoplasm (Stephens et al., 2011, Forment et al., 2012). Chromoplexy frequently involves fewer rearrangements than the "catastrophic" chromothripsis defined by Stephens et al. (2011) but may continue throughout tumor development. Our analysis of breakpoint locations in ETS⁺ tumors suggests that chromoplexy in this setting may be linked to proposed transcriptional DNA-damaging processes (Lin et al., 2009), potentially related to androgen receptor signaling. We stress that this hypothesis awaits experimental validation, which could involve fluorescence in situ hybridization (FISH) or chromosome conformation capture before and after inducing a predicted colocalizing event (e.g., testosterone exposure in prostate epithelial cells). Our findings align with the observation that ERG-overexpressing cancer cells accumulate DNA damage and are sensitive to poly ADP-ribose polymerase inhibition (Brenner et al., 2011). However, chromoplexy is active prior to ETS gene fusions and generates *ERG* fusions in many instances.

Whole-genome analysis also clarified the chronology of oncogenic events in prostate cancer progression, driven, in part, by chromoplexy. Genome-wide sequence coverage of germline SNPs allowed us to identify DNA lesions that arose after the founder clone was established. Subsequently, we demonstrated a progression of events within primary tumors that expands upon array-based SCNA co-occurrence studies (Demichelis et al., 2009). A consensus path of tumor evolution begins with events such as the loss of *NKX3-1* or the fusion of *TMPRSS2* and *ERG*. The path proceeds with the loss of *CDKN1B*, *TP53* and *PTEN*, and other progression-associated lesions. We found that the histological grade of cancer may partially reflect its progression down this path.
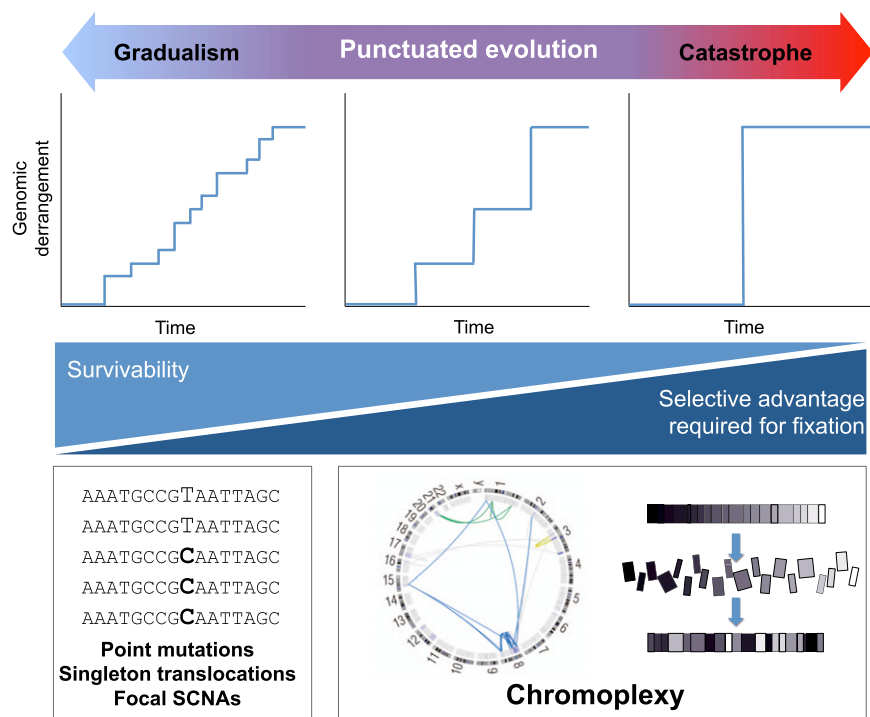
Figure 7. A Continuum Model for the Genomic Evolution of Prostate Cancer
Oncogenic aberrations may accumulate in cancer genomes gradually (left), by punctuated progression (middle), or in a single catastrophic event (right). Chromoplectic rearrangements and deletions induce a modest to large degree of genomic derangement over several successive events. As indicated at the bottom, larger-scale rearrangements that affect broader swaths of the genome may be more difficult for a cell to survive in and may tend to require co-occurring oncogenic lesions to become fixed in a tumor.
Also see Figure S7.

the "catastrophic" end may require fewer events and could progress more quickly, because each event could disrupt multiple cancer-constraining processes. At the same time, catastrophic events that cover diffuse genomic territory are more liable to disrupt essential or beneficial genes, thus imparting a selective disadvantage to malignant and premalignant clones that sustain such events. Consequently, the model predicts that survivable chromoplexy (particularly near the catastrophic regime) is likely to involve oncogenic alterations that compensate for the incidental inactivation of essential genes (Figure 7). This prediction accords with the observation that most tumors show disruption of one or more putative prostate cancer genes within a chain. Moreover, this model raises the possibility that the disruption of putative cancer genes by chromoplexy may heighten the probability that such genes represent "driver" events for that particular tumor. If so, this framework may portend important implications for the use of WGS in diagnostic and clinical studies.

In summary, this study highlights the potential for WGS data to capture aspects of the "molecular archeology" of cancer development that are missed by gene- or exome-level sequencing. The characterization of clonal progression and chromoplexy in emerging large panels of cancer genomes may provide insights into tumor initiation and progression that impact cancer detection, prevention, and therapy.

EXPERIMENTAL PROCEDURES

Sample Acquisition
Prostate tumors were obtained under protocols approved by the Broad Institute Institutional Review Board from consented patients undergoing radical prostatectomy or excision of soft-tissue metastases (PR-4240 and PR-7520). Normal DNA was derived either from histologically benign prostate tissue or peripheral blood cells. Specimens were collected at Weill Cornell Medical College by A.T. and at various medical centers in Western Australia in conjunction with Uropath Pty (Perth, Australia).

DNA Library Construction and WGS
Tissue cores were extracted from cancerous foci of frozen or paraffin-embedded tumor nodules. After tissue homogenization and lysis, DNA was extracted and assessed for quality (Berger et al., 2011). After library construction,

A Continuum Model for Tumor Evolution
Tumorigenesis is classically understood to progress by a gradual accumulation of oncogenic alterations in the genome of a pre-cancerous cell. This textbook view was recently challenged by the discovery of chromothripsis, in which catastrophic rearrangements are incurred by "shattering" and reassembly of focal regions of the genome (Forment et al., 2012; Rausch et al., 2012; Stephens et al., 2011).

We propose an expanded model for the evolution of prostate cancer, which may also apply to other cancers (Figure 7). As classically understood, passenger and driver alterations can accumulate in a cancer genome gradually over numerous cell divisions, through point mutations, simple translocations, and focal copy number alterations. On the opposite end of the spectrum, extreme instances of chromothripsis can induce massive (albeit relatively localized) DNA damage at once, often with oncogenic consequences (Rausch et al., 2012; Stephens et al., 2011). Between these two extremes lies a broad continuum across which chromoplexy may often restructure cancer genomes. We propose that oncogenic events along this continuum reflect "punctuated" tumor evolution, drawing an analogy from the observation that the punctuated evolution of species may occur rapidly between periods of relative mutational equilibrium (Gould and Eldrige, 1977). By analogy, a tumor genome may sustain considerable damage over several sequential and punctuated events. Importantly, this framework accords with the observation that chromoplexy events (1) are common, (2) may involve a wide-ranging number of rearrangements, and (3) may continue after the deletion of cancer-initiating lesions such as *NKX3-1* (Figure S7).

A cancer might operate at any point along the continuum of progression at a given time. Tumors that develop primarily at

paired-end sequencing reads of 101 nucleotides were generated with an Illumina GAIIx instrument. Sequencing data were aligned to the hg19 human reference genome with BWA (Li and Durbin, 2009) and processed by the Picard pipelines (http://picard.sourceforge.net).

Detection and Validation of Genomic Alterations

Somatic point mutations, small indels, and rearrangements were detected by comparison of tumor and paired normal genome sequences with MuTect (Cibulskis et al., 2013), Indelocator (http://broadinstitute.org/cancer/cga/), and dRanger (Berger et al., 2011), respectively. dRanger was used as described previously (Berger et al., 2011), except high-confidence rearrangements required support from four or more high-quality sequencing reads and were filtered against a panel of 176 normal tissue genomes. Somatic fusion breakpoints were located at base-pair resolution where possible with the BreakPointer algorithm (Drier et al., 2013). Paired-end reads from rearrangements affecting cancer genes or participating in long chains were inspected manually. A subset of rearrangements was validated by resequencing and/or PCR amplification of tumor and normal DNA.

Chromosomal Copy Number Profiling

Segmented copy number profiles were generated from Affymetrix SNP 6.0 human SNP microarray (Affymetrix, Santa Clara, CA, USA) data as described previously (Barbieri et al., 2012). Sites of significant recurrent copy number alterations were identified by GISTICv2 (Mermel et al., 2011) with a $\log_2$ threshold of ±0.1 for amplification and deletion signals.

Identification of Chained Rearrangements and Deletions

The ChainFinder algorithm was implemented to detect chromoplexy from the combined analysis of somatic fusion breakpoints and segmented copy number profiles. ChainFinder considers breakpoints as nodes in a graph that are connected by edges corresponding to (1) fusions, (2) deletion bridges, or (3) breakpoint adjacency that deviates significantly from the null model of independent breakpoints (Figure S3). Over several steps, the algorithm evaluates potential deletion bridges and adjacently mapped breakpoints to assign rearrangements to chains.

First, ChainFinder identifies potential deletion bridges by searching for distinct breakpoints that plausibly correspond to the boundaries of deletion events observed in copy number profiles. Next, a statistical analysis of all nearest neighbor breakpoint pair distances identifies chain-like distributions of rearrangements. The local rate of expected independent breaks per nucleotide (μ) is calculated for 1 Mb genomic windows on the basis of (1) the rearrangement frequency within the window across a panel of tumor genomes and (2) the total number of breaks in the genome under consideration. Given μ, ChainFinder models the probability (P_{XY}) of observing two independently arising fusion breakpoints within the observed distance (L) of each other on the reference genome (i.e., the p value under the null model of independent breaks):

$$P_{XY} = 1 - (1 - 2\mu)^L$$

If P_{XY} is rejected with a false-discovery rate of 10^{-2} (Benjamini and Hochberg, 1995), then the corresponding breakpoints are linked in a chain.

The graph is also searched for closed paths (cycles) through nodes and connecting edges. For each cycle, all possible scenarios are considered by which the contained breakpoints could have arisen independently. Breakpoints in the cycle are assigned to the same chain if p values for every scenario can be rejected with a family-wise error rate (FWER) below 10^{-2}.

Lastly, the graph is finalized by assigning additional sets of edges corresponding to deletion bridges that could not be assigned uniquely in the first step. The search maximizes the number of deletion bridges in cycles to find solutions that account most fully for the overlap of fusion breakpoints with boundaries of deletion segments on the reference genome. A complete description of ChainFinder is provided in Extended Experimental Procedures. ChainFinder can be downloaded at http://broadinstitute.org/cancer/cga/chainfinder.

Assessment of Stromal DNA Admixture and Clonality

We used the sequence coverage from germline SNPs at sites of somatic deletion to assess levels of stromal DNA admixture in sequenced samples and to infer the clonal status of mutations and deletions by applying CLONET (CLONality Estimate in Tumors; Extended Experimental Procedures). We assessed the allelic fractions of SNP reads within hemizygously-deleted DNA in order to determine the apparent proportions of DNA from normal cells at the deleted locus. Deletions with the lowest apparent proportions of normal DNA reads were considered clonal. For all other deletions, we estimated the percentage of tumor cells harboring the deletion to infer the clonality of the lesion using simulation-based error estimates. For point mutations, the tumor allelic fraction was corrected for stromal DNA admixture, and subclonality was inferred when the corrected fraction differed significantly from the expected value. Lesions present in 80% of cancer cells or less were considered subclonal.

Statistical Analyses

Quantitative comparisons of groups (e.g., numbers of rearrangements or SCNAs) were conducted with a Mann-Whitney test unless indicated otherwise. Box plots indicate median values and middle quartiles.

SUPPLEMENTAL INFORMATION

Supplemental Information includes Extended Experimental Procedures, seven figures, and seven tables and can be found with this article online at http://dx.doi.org/10.1016/j.cell.2013.03.021.

REFERENCES

Baca, S.C., and Garraway, L.A. (2012). The genomic landscape of prostate cancer. Front. Endocrinol. (Lausanne) *3*, 69.

Barbieri, C.E., Baca, S.C., Lawrence, M.S., Demichelis, F., Blattner, M., Theurillat, J.P., White, T.A., Stojanov, P., Van Allen, E., Stransky, N., et al. (2012). Exome sequencing identifies recurrent SPOP, FOXA1 and MED12 mutations in prostate cancer. Nat. Genet. *44*, 685–689.

Benjamini, Y., and Hochberg, Y. (1995). Controlling the false discovery rate: a practical and powerful approach to multiple testing. J.R. Stat. Soc. *57*, 289–300.

Berger, M.F., Lawrence, M.S., Demichelis, F., Drier, Y., Cibulskis, K., Sivachenko, A.Y., Sboner, A., Esgueva, R., Pflueger, D., Sougnez, C., et al.

(2011). The genomic complexity of primary human prostate cancer. Nature *470*, 214–220.

Bhatia-Gaur, R., Donjacour, A.A., Sciavolino, P.J., Kim, M., Desai, N., Young, P., Norton, C.R., Gridley, T., Cardiff, R.D., Cunha, G.R., et al. (1999). Roles for Nkx3.1 in prostate development and cancer. Genes Dev. *13*, 966–977.

Brenner, J.C., Ateeq, B., Li, Y., Yocum, A.K., Cao, Q., Asangani, I.A., Patel, S., Wang, X., Liang, H., Yu, J., et al. (2011). Mechanistic rationale for inhibition of poly(ADP-ribose) polymerase in ETS gene fusion-positive prostate cancer. Cancer Cell *19*, 664–678.

Burrow, A.A., Marullo, A., Holder, L.R., and Wang, Y.H. (2010). Secondary structure formation and DNA instability at fragile site FRA16B. Nucleic Acids Res. *38*, 2865–2877.

Carter, S.L., Cibulskis, K., Helman, E., McKenna, A., Shen, H., Zack, T., Laird, P.W., Onofrio, R.C., Winckler, W., Weir, B.A., et al. (2012). Absolute quantification of somatic DNA alterations in human cancer. Nat. Biotechnol. *30*, 413–421.

Chen, Z., Trotman, L.C., Shaffer, D., Lin, H.K., Dotan, Z.A., Niki, M., Koutcher, J.A., Scher, H.I., Ludwig, T., Gerald, W., et al. (2005). Crucial role of p53-dependent cellular senescence in suppression of Pten-deficient tumorigenesis. Nature *436*, 725–730.

Cibulskis, K., Lawrence, M.S., Carter, S.L., Sivachenko, A., Jaffe, D., Sougnez, C., Gabriel, S., Meyerson, M., Lander, E.S., and Getz, G. (2013). Sensitive detection of somatic point mutations in impure and heterogeneous cancer samples. Nat. Biotechnol. *31*, 213–219.

De, S., and Michor, F. (2011). DNA replication timing and long-range DNA interactions predict mutational landscapes of cancer genomes. Nat. Biotechnol. *29*, 1103–1108.

Demichelis, F., Setlur, S.R., Beroukhim, R., Perner, S., Korbel, J.O., Lafargue, C.J., Pflueger, D., Pina, C., Hofer, M.D., Sboner, A., et al. (2009). Distinct genomic aberrations associated with ERG rearranged prostate cancer. Genes Chromosomes Cancer *48*, 366–380.

Ding, Z., Wu, C.J., Chu, G.C., Xiao, Y., Ho, D., Zhang, J., Perry, S.R., Labrot, E.S., Wu, X., Lis, R., et al. (2011). SMAD4-dependent barrier constrains prostate cancer growth and metastatic progression. Nature *470*, 269–273.

Drier, Y., Lawrence, M.S., Carter, S.L., Stewart, C., Gabriel, S.B., Lander, E.S., Meyerson, M., Beroukhim, R., and Getz, G. (2013). Somatic rearrangements across cancer reveal classes of samples with distinct patterns of DNA breakage and rearrangement-induced hypermutability. Genome Res. *23*, 228–235.

Emmert-Buck, M.R., Vocke, C.D., Pozzatti, R.O., Duray, P.H., Jennings, S.B., Florence, C.D., Zhuang, Z., Bostwick, D.G., Liotta, L.A., and Linehan, W.M. (1995). Allelic loss on chromosome 8p12-21 in microdissected prostatic intra-epithelial neoplasia. Cancer Res. *55*, 2959–2962.

Fearon, E.R., and Vogelstein, B. (1990). A genetic model for colorectal tumorigenesis. Cell *61*, 759–767.

Forment, J.V., Kaidi, A., and Jackson, S.P. (2012). Chromothripsis and cancer: causes and consequences of chromosome shattering. Nat. Rev. Cancer *12*, 663–670.

Gaspar-Maia, A., Alajem, A., Polesso, F., Sridharan, R., Mason, M.J., Heidersbach, A., Ramalho-Santos, J., McManus, M.T., Plath, K., Meshorer, E., and Ramalho-Santos, M. (2009). Chd1 regulates open chromatin and pluripotency of embryonic stem cells. Nature *460*, 863–868.

Gould, S.J., and Eldrige, N. (1977). Punctuated equilibria: the tempo and mode of evolution reconsidered. Paleobiology *3*, 115–151.

Grasso, C.S., Wu, Y.M., Robinson, D.R., Cao, X., Dhanasekaran, S.M., Khan, A.P., Quist, M.J., Jing, X., Lonigro, R.J., Brenner, J.C., et al. (2012). The mutational landscape of lethal castration-resistant prostate cancer. Nature *487*, 239–243.

Haffner, M.C., Aryee, M.J., Toubaji, A., Esopi, D.M., Albadine, R., Gurel, B., Isaacs, W.B., Bova, G.S., Liu, W., Xu, J., et al. (2010). Androgen-induced TOP2B-mediated double-strand breaks and prostate cancer gene rearrangements. Nat. Genet. *42*, 668–675.

Halvorsen, O.J., Haukaas, S.A., and Akslen, L.A. (2003). Combined loss of PTEN and p27 expression is associated with tumor cell proliferation by Ki-67 and increased risk of recurrent disease in localized prostate cancer. Clin. Cancer Res. *9*, 1474–1479.

Huang, S., Gulzar, Z.G., Salari, K., Lapointe, J., Brooks, J.D., and Pollack, J.R. (2012). Recurrent deletion of CHD1 in prostate cancer with relevance to cell invasiveness. Oncogene *31*, 4164–4170.

Jemal, A., Bray, F., Center, M.M., Ferlay, J., Ward, E., and Forman, D. (2011). Global cancer statistics. CA Cancer J. Clin. *61*, 69–90.

Kanehisa, M., Goto, S., Sato, Y., Furumichi, M., and Tanabe, M. (2012). KEGG for integration and interpretation of large-scale molecular data sets. Nucleic Acids Res. *40*(Database issue), D109–D114.

Kumar, A., White, T.A., MacKenzie, A.P., Clegg, N., Lee, C., Dumpit, R.F., Coleman, I., Ng, S.B., Salipante, S.J., Rieder, M.J., et al. (2011). Exome sequencing identifies a spectrum of mutation frequencies in advanced and lethal prostate cancers. Proc. Natl. Acad. Sci. USA *108*, 17087–17092.

Li, H., and Durbin, R. (2009). Fast and accurate short read alignment with Burrows-Wheeler transform. Bioinformatics *25*, 1754–1760.

Lin, C., Yang, L., Tanasa, B., Hutt, K., Ju, B.G., Ohgi, K., Zhang, J., Rose, D.W., Fu, X.D., Glass, C.K., and Rosenfeld, M.G. (2009). Nuclear receptor-induced chromosomal proximity and DNA breaks underlie specific translocations in cancer. Cell *139*, 1069–1083.

Liu, W., Lindberg, J., Sui, G., Luo, J., Egevad, L., Li, T., Xie, C., Wan, M., Kim, S.T., Wang, Z., et al. (2012). Identification of novel CHD1-associated collaborative alterations of genomic structure and functional assessment of CHD1 in prostate cancer. Oncogene *31*, 3939–3948.

Mermel, C.H., Schumacher, S.E., Hill, B., Meyerson, M.L., Beroukhim, R., and Getz, G. (2011). GISTIC2.0 facilitates sensitive and confident localization of the targets of focal somatic copy-number alteration in human cancers. Genome Biol. *12*, R41.

Nik-Zainal, S., Van Loo, P., Wedge, D.C., Alexandrov, L.B., Greenman, C.D., Lau, K.W., Raine, K., Jones, D., Marshall, J., Ramakrishna, M., et al.; Breast Cancer Working Group of the International Cancer Genome Consortium. (2012). The life history of 21 breast cancers. Cell *149*, 994–1007.

Perner, S., Demichelis, F., Beroukhim, R., Schmidt, F.H., Mosquera, J.-M., Setlur, S., Tchinda, J., Tomlins, S.A., Hofer, M.D., Pienta, K.G., et al. (2006). TMPRSS2:ERG fusion-associated deletions provide insight into the heterogeneity of prostate cancer. Cancer Res. *66*, 8337–8341.

Perner, S., Mosquera, J.M., Demichelis, F., Hofer, M.D., Paris, P.L., Simko, J., Collins, C., Bismar, T.A., Chinnaiyan, A.M., De Marzo, A.M., and Rubin, M.A. (2007). TMPRSS2-ERG fusion prostate cancer: an early molecular event associated with invasion. Am. J. Surg. Pathol. *31*, 882–888.

Rausch, T., Jones, D.T., Zapatka, M., Stütz, A.M., Zichner, T., Weischenfeldt, J., Jäger, N., Remke, M., Shih, D., Northcott, P.A., et al. (2012). Genome sequencing of pediatric medulloblastoma links catastrophic DNA rearrangements with TP53 mutations. Cell *148*, 59–71.

Shen, M.M., and Abate-Shen, C. (2010). Molecular genetics of prostate cancer: new prospects for old challenges. Genes Dev. *24*, 1967–2000.

Stephens, P.J., Greenman, C.D., Fu, B., Yang, F., Bignell, G.R., Mudie, L.J., Pleasance, E.D., Lau, K.W., Beare, D., Stebbings, L.A., et al. (2011). Massive genomic rearrangement acquired in a single catastrophic event during cancer development. Cell *144*, 27–40.

Sun, C., Dobi, A., Mohamed, A., Li, H., Thangapazham, R.L., Furusato, B., Shaheduzzaman, S., Tan, S.H., Vaidyanathan, G., Whitman, E., et al. (2008). TMPRSS2-ERG fusion, a common genomic alteration in prostate cancer activates C-MYC and abrogates prostate epithelial differentiation. Oncogene *27*, 5348–5353.

Tomlins, S.A., Rhodes, D.R., Perner, S., Dhanasekaran, S.M., Mehra, R., Sun, X.W., Varambally, S., Cao, X., Tchinda, J., Kuefer, R., et al. (2005). Recurrent fusion of TMPRSS2 and ETS transcription factor genes in prostate cancer. Science *310*, 644–648.

Tomlins, S.A., Laxman, B., Dhanasekaran, S.M., Helgeson, B.E., Cao, X., Morris, D.S., Menon, A., Jing, X., Cao, Q., Han, B., et al. (2007). Distinct classes of chromosomal rearrangements create oncogenic ETS gene fusions in prostate cancer. Nature *448*, 595–599.